frontiers | Frontiers in Mechanical Engineering

TYPE Original Research
PUBLISHED 22 August 2022
DOI 10.3389/fmech.2022.931377

OPEN ACCESS

EDITED BY
Stephen Anthony Ciatti,
Independent researcher, United States

REVIEWED BY
Haifeng Liu,
Tianjin University, China
Luca Marchitto,
CNR-Istituto di Scienze e Tecnologie per l'Energia e la Mobilità Sostenibili (STEMS), Italy

*CORRESPONDENCE
Ji-Woong Park,
ji-woong.park@aramcoamericas.com

SPECIALTY SECTION
This article was submitted to Engine and Automotive Engineering, a section of the journal Frontiers in Mechanical Engineering

RECEIVED 28 April 2022
ACCEPTED 11 July 2022
PUBLISHED 22 August 2022

CITATION
Park J-W, Jouzdani S, Tzanetakis T, Schmidt H, Atkinson W, Naber J, Pei Y, Tao F, Garg R, Langenderfer D, Zhang Y and Som S (2022), Experimental diesel spray characterization of the medium-duty injector with single- and multi-hole nozzle configurations under non-reacting, non-vaporizing conditions. *Front. Mech. Eng* 8:931377. doi: 10.3389/fmech.2022.931377

Experimental diesel spray characterization of the medium-duty injector with single- and multi-hole nozzle configurations under non-reacting, non-vaporizing conditions

Ji-Woong Park[1,2]*, Shirin Jouzdani[3], Tom Tzanetakis[1], Henry Schmidt[3], William Atkinson[3], Jeffrey Naber[3], Yuanjiang Pei[1], Feng Tao[4], Rajesh Garg[4], David Langenderfer[4], Yu Zhang[1] and Sibendu Som[2]

[1]Aramco Americas: Aramco Research Center–Detroit, Novi, MI, United States, [2]Argonne National Laboratory, Lemont, IL, United States, [3]Michigan Technological University, Houghton, MI, United States, [4]Cummins Inc., Columbus, IN, United States

Characteristics of diesel sprays injected through Cummins medium-duty ISB injectors were studied experimentally in an optically accessible constant-volume combustion vessel. The experiments were performed with ultra-low-sulfur diesel (ULSD) under non-reacting and non-vaporizing conditions, including different ambient gas densities (23–65 kg/m^3), injection pressures (500–1,500 bar), and injection duration times (0.5–1.5 ms). The ambient temperature of the vessel was maintained at a room temperature of 313 K for all the tests. A systematic comparison was made between single-hole (SH) and multi-hole (MH) injector configurations. A plume-to-plume variation in spray penetration length was observed for various operating conditions. A substantial deviation was observed for a specific hole against the averaged plume, indicating that arbitrary selection of the plume index may result in inaccurate spray characterization of the MH injector. The penetration length of the MH injector was shorter than that of the SH injector under the same operating conditions, indicating that a spray model calibrated on SH injector data may not accurately predict the transient spray behavior of the MH injector in practical engine simulations. A square-root correlation of the spray penetration length was applied for both the SH and MH injectors. The spray penetration length and dispersion angles of the ISB SH injector were also compared with those of the heavy-duty Cummins ISX SH injector. While the ISX SH injector showed a faster penetration than the ISB SH injector, the dispersion angle was similar. The differences in spray penetration between ISB and ISX injectors followed the expected trend based on their nozzle hole diameters.

KEYWORDS

diesel, spray characterization, multi-hole injector, single-hole injector, non-reacting, non-vaporizing

1 Introduction

Diesel fuel has been widely used in various transportation sectors, including marine, agricultural, and heavy-duty on-road applications. The reason it provides a large portion of the energy supply in the transportation sector is mostly attributed to its high energy density, as well as the well-established distribution network for refueling (U.S. Energy Information Administration, 2021; International Energy Agency, 2021). However, strict emission regulations with increased demand for reduced fuel consumption have prompted researchers to seek next-generation diesel engines that improve fuel efficiency and reduce pollutant emissions. Advanced injector and combustion technologies include, but are not limited to, high-pressure common-rail systems (Sellnau et al., 2019), exhaust-gas recirculation (EGR) (D'Ambrosio and Ferrari, 2015), thermal barrier coatings (Garcia, 2021), advanced air handling systems with Miller cycle intake valve strategies (Garcia, 2021), multiple injections strategies (Choi and Park, 2022; Liu et al., 2022), and piston-bowl shape optimization (Subramanian et al., 2016; Guo Z. et al., 2020). To improve thermal efficiency and reduce emissions, an accurate understanding of spray characterization is critical because it determines fuel-air mixing and piston/wall-wetting phenomena (Kook and Pickett, 2012), which consequently affect combustion and emission processes.

Extensive experimental and computational studies on automotive injector sprays have been performed by several research groups (e.g., Siebers, 1998; Siebers, 1999; Arcoumanis et al., 2000; Siebers and Higgins, 2001; Kennaird et al., 2002; Senecal et al., 2003; Tang et al., 2018; Chen et al., 2019; Tzanetakis et al., 2021; Yi et al., 2021; Engine Combustion Network (ECN), 2022; Tzanetakis et al., 2022). Prior to the end of the 1990s, spray characterization was performed by varying the injection strategies, including injection pressure, back chamber pressure, orifice diameter, and the number of orifices (Naber and Siebers, 1996; Siebers, 1998; Tennison et al., 1998; Siebers, 1999; Arcoumanis et al., 2000; Siebers and Higgins, 2001; Kennaird et al., 2002). Since then, extensive work has been performed in this area, much of it by the Engine Combustion Network (ECN) (Engine Combustion Network (ECN), 2022). In 2011, the first proceeding of ECN was initiated with a particular focus on internal nozzle flow, near-field (i.e., nozzle tip) spray behavior, vaporizing sprays, ignition, flame morphology, and emissions. Through collaboration among a variety of research organizations, the ECN has established a well-organized database covering a wide range of operating conditions, injector specifications, experimental facility effects, and so on. These data are available online and have been widely used as a validation set to develop predictive diesel spray models used for computational fluid dynamics (CFD) simulations (Pastor et al., 2012; Pomraning et al., 2014; Pei et al., 2015; Payri et al., 2016a; Pastor et al., 2018; Tang et al., 2018; Battistoni et al., 2019; Guo H. et al., 2020; García-Oliver et al., 2020). The ECN has considered various diesel research nozzle configurations (Sprays A, B, C, and D) based on a common rail fuel injector generated by Bosch (Engine Combustion Network (ECN), 2022). Single-hole (SH) injectors of Sprays A, C, and D have different nominal orifice diameters of 90, 200, and 186 μm, respectively. The Spray B configuration is a 3-hole injector with an orifice diameter of 90 μm, the same diameter as Spray A. The specifications of ECN diesel research injectors are briefly summarized in Table 1. These variations allowed systematic experimental investigation of the impact of multiple holes (Spray A vs. B) (Pickett et al., 2013; Jung et al., 2015; Payri et al., 2016a) and nozzle diameter (Spray A vs. C and D) on spray characterization (Pastor et al., 2012; Payri et al., 2014; Payri et al., 2016b; Pastor et al., 2018; García-Oliver et al., 2020). Several research institutions have studied these injectors using different measuring techniques. However, the number of holes in a practical engine is larger than the number used in ECN research injectors [e.g., 7 holes (Jin et al., 2020) or even more than 10 holes (Dong et al., 2016; Zhai et al., 2021a)]. Therefore, the sprays from a practical injector with a more representative number of nozzle holes exposed to engine-relevant operating conditions need to be investigated.

In addition to the ECN-based research injectors, many research groups have investigated the spray characterization of production multi-hole (MH) injectors (Dong et al., 2016; Jin et al., 2020; Zhai et al., 2021a) and compared them to SH injectors (Moon et al., 2015; Jin et al., 2020). A few studies using the production MH injectors are summarized in Table 1. Dong et al. (2016) investigated the effects of the nozzle configuration (SH and MH) and injection quantity (or injection duration) both experimentally and numerically. The SH injector showed a longer penetration length than the MH injector, while the MH injector showed a larger spray cone angle of the individual plume of interest than the SH injector. CFD simulations were carried out using the commercial software AVL FIRE, Version 2013 (AVL FIRE, 2013) to further provide the internal flow characteristics. Simulation results showed that the SH injector exhibited symmetric film-type cavitation, while the MH injector showed asymmetric cavitation behavior due to the internal spiral and streamwise counter-rotating flow. Jin et al. (2020) also compared the SH and MH injectors in a vaporizing spray condition at an ambient temperature of 800 K. Under the same rail pressure, the sac pressure of the SH injector increased faster than the MH injector, resulting in a larger velocity at the hole exit and, thereby, faster

TABLE 1 Specification of diesel injectors used by the ECN, in the literature and this study.

Category	Name	Nozzle diameter [μm]	Number of holes	Comments
ECN Research Injectors	Spray A	90	1	Bosch generation 2.4 Benajes et al. (2013), Payri et al. (2014), Yao et al. (2017), Engine Combustion Network (ECN) (2022)
	Spray B	90	3	Bosch generation 2.4 Jung et al. (2015), Eagle et al. (2016), Battistoni et al. (2019), Engine Combustion Network (ECN) (2022)
	Spray C	200	1	Bosch 3-22 Payri et al. (2019), Yasutomi et al. (2020), Guo H. et al. (2020), Engine Combustion Network (ECN) (2022)
	Spray D	186	1	Bosch 3-22 Payri et al. (2014), Yasutomi et al. (2020), Engine Combustion Network (ECN) (2022)
Production Injectors	ISX	186	8	Cummins Heavy-duty
	ISB	146	8	Cummins Medium-duty
	Zhai (2020)	70/101/133	10	Denso G4s Solenoid Injector Zhai et al. (2021a)
	Jin (2021)	123	7	Denso Corporation Injector Jin et al. (2020)

TABLE 2 Various experimental scenarios for spray characterization.

Scenario	Non-reacting/Non-vaporizing	Non-reacting/Vaporizing	Reacting/Vaporizing
Label	NR/NV	NR/V	R/V
Oxygen availability	No	No	Yes
Ambient Temperature	Low	High	High
Relevant Physics	Break-up/Atomization	Break-up/Atomization, Vaporization	Break-up/Atomization, Vaporization, Ignition, Combustion, Emissions
References	Tang et al. (2017), Zhao et al. (2017)	Zhang et al. (2017), Tzanetakis et al. (2022)	Siebers and Higgins (2001), Payri et al. (2016a), Tang et al. (2016), Tang et al. (2018), Chen et al. (2019), Yi et al. (2021)

vapor penetration due to the enhanced air entrainment. By decreasing the injection pressure of the SH injector, they found that the SH and MH injectors showed similar injection rate profiles and similar vapor penetration. Interestingly, even if both types of injectors observed similar injection rates, nozzle exit velocity, and spray tip penetration, the SH injector showed a smaller angle than the MH injector, indicating the crucial role of internal nozzle flow on spray characteristics. Zhai et al. (2021a) investigated the effect of the nozzle hole diameter (70, 101, and 133 μm) on non-evaporating spray characteristics under high injection pressures (i.e., 1,000, 2,000, and 3,000 bar). At the same injection pressure, the larger diameters showed faster penetration and a slightly larger spray angle due to the larger effective nozzle flow area, momentum, turbulent energy, and enhanced entrainment capacity. In contrast, for the same injector diameter (70 μm), the higher injection pressures showed faster penetration while the spray angle remained constant. Also, better air-fuel mixing was observed in high-pressure conditions due to the enhanced entrainment rate. Furthermore, several experimental (Moon et al., 2015; Huang et al., 2017; Torelli et al., 2018) and numerical (Torelli et al., 2017a; Zhao et al., 2017) studies were performed to elucidate the internal nozzle flow and eccentric needle motion effects on MH diesel spray injectors. As discussed above, while extensive work has been conducted using the ECN-based research injectors, the spray behavior of practical MH injectors with a larger number of holes and different orifice diameters may be quite complex. As such, the spray characterization of a practical or production MH injector and comparison with a representative SH injector are needed.

It is also worth noting that the spray penetration length can be measured in vaporizing/non-vaporizing and reacting/non-reacting conditions depending on the ambient temperature and oxygen availability, which are all summarized in Table 2. The reacting and vaporizing condition (R/V) is a more practical engine-relevant condition than the other two cases, but it inherently involves complex physics, including break-up/atomization, vaporization, combustion, and their interactions. In contrast, the non-reacting/non-vaporizing condition (NR/NV) can be made by filling the chamber with nitrogen at a low ambient temperature, less than the initial boiling point of the injected liquid. Therefore, this operating condition mainly involves spray break-up/atomization processes with minimal vaporization and combustion effects. Experimental data measured in these scenarios can provide valuable insight for investigating spray characterization. Also, the measured experimental data can be a useful input for the spray break-

up model, evaporation model, and combustion model validations to develop a predictive engine computational model. As a baseline and first step, the current study focuses on the NR/NV condition, while the other scenarios will be reported in future works.

In prior works (Dong et al., 2016; Jin et al., 2020; Zhai et al., 2021a), a specific plume of interest was chosen to represent the spray penetration of MH injectors for easier optical access to characterize the spray behavior. Due to complex internal nozzle flows and cavitation phenomena, diesel MH injectors may experience plume-to-plume spray variations (Nesbitt et al., 2011; Jung et al., 2015; Huang et al., 2017; Torelli et al., 2018). Thus, an arbitrarily selected plume of interest may not properly capture nominal spray behavior, which is necessary for predictive CFD model development. Also, the effects of nozzle-hole diameter on the spray penetration and its comparison between SH and MH practical injectors are of great interest for developing advanced diesel combustion strategies.

In the current study, the experimental spray characterization was performed by measuring the spray penetration length of the MH injector of a Cummins medium-duty ISB production engine. The plume-to-plume variation is discussed first, followed by a parametric evaluation of the spray penetration length under a wide range of engine-relevant conditions. The ISB SH injector's spray penetration length and dispersion angle were compared with those of a heavy-duty ISX SH injector to evaluate the different injector specifications (e.g., nozzle-hole diameter, etc.). Finally, the spray penetration length of the MH injector was compared with that of the SH injector to highlight the difference between them. An empirical spray penetration correlation relating to the SH and MH injectors is also presented. The experimental measurements and analysis data deduced from the current work provide detailed information on the spray behavior under practical engine configurations and useful input to further validate and improve the spray model.

2 Materials and methods

2.1 Fuel specifications

The properties of the certified diesel fuel, ultra-low-sulfur diesel (ULSD), used for the experiment were measured based on the fuel sample from Haltermann Solutions (Tzanetakis et al., 2022) and are summarized in Table 3.

TABLE 3 Fuel properties (measured based on the sample fuel from Haltermann solutions).

Property	Units	ULSD	Method
Density	kg/m^3	848	ASTM D4052
Viscosity[a]	cSt	2.6	ASTM D445
Initial boiling point (IBP)	°C	173.3	ASTM D86
T10	°C	214.4	ASTM D86
T50	°C	267.8	ASTM D86
T90	°C	315.0	ASTM D86
Full boiling point (FBP)	°C	347.0	ASTM D86
Wear scar diameter (WSD^2)	µm	570	ASTM D6079
Saturates	% Vol	71	ASTM D1319
Olefins	% Vol	1	ASTM D1319
Aromatics	% Vol	28	ASTM D1319
Sulfur	ppm (m)	8	ASTM D5453
H/C ratio	mol/mol	1.82	ASTM D5291
Lower heating value (LHV)	MJ/kg	42.83	ASTM D240
Cetane number (CN)	—	44.2	ASTM D613

[a]Measured at 40°C.
[b]Measured at 60°C.

2.2 Experimental setup

A constant-volume (CV) combustion chamber with an optically accessible window was utilized where the vessel volume was 1 L. The charge temperature was set to 40°C, which is below the initial boiling point (IBP) of 173°C, as shown in Table 3, to minimize the vaporization.

The liquid spray penetration length can be measured using different techniques, including shadowgraph (Tang et al., 2017; Zhang et al., 2017), Mie scattering (Zhang et al., 2017), and diffuse back-illumination (DBI) (Pickett et al., 2013; Zhai et al., 2021b). While these techniques can be used to measure for the SH injector, only Mie scattering is applicable for the MH injector because we aimed to measure the front view images rather than the side view. Liquid phase spray was visualized using the Mie-scattering technique as shown in the schematic experimental apparatus seen in Figure 1(A–B). By scattering light off the fuel droplets using two digital pulsed light-emitting diodes (LEDs), the liquid portion of the spray could be visualized and captured with a high-speed digital camera (FASTCAM SA1.1). Details of measurement techniques can be found in several studies (Nesbitt et al., 2011; Zhang et al., 2017). The injector was installed backside of the CV and could be observed from the front and side observation windows. The spray penetration length of the SH injector was measured from the side observation window, while that of the MH injector was measured from the front view with consideration of the angled spray based on the injector orientation.

2.3 Injectors

Specifications and schematics of the SH and MH injectors are summarized in Table 4 and Figure 1(C–D), respectively. The MH injector was a Cummins XPI ISB product injector, which has eight nozzle holes and an umbrella spray angle of 141°. The SH injector was specifically designed for this study, being intended to

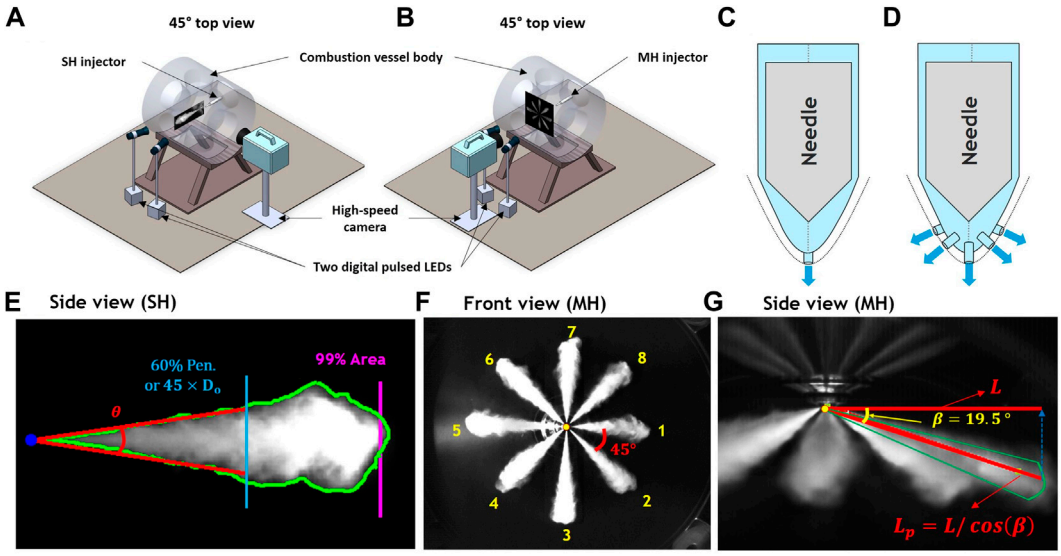

FIGURE 1
Optical setup of the Mie-scattering imaging system of **(A)** single-hole and **(B)** multi-hole injectors for the non-reacting, non-vaporizing tests. Schematic of **(C)** single- and **(D)** multi-hole injectors. **(E)** The side view of a single-hole (SH) injector with different definitions of spray penetration lengths (99% area) and dispersion angles (60% pen or 45×D_o). The **(F)** front and **(G)** side views of the multi-hole (MH) injector with plume index by the determination of the actual penetration length (L_p) from the visualized penetration length (L).

TABLE 4 Injector specification of the medium-duty ISB single- and multi-hole injectors.

Medium-duty ISB injector	Single-hole	Multi-hole
Manufacturer	Cummins	
Type of Injector	Extreme pressure injector (XPI)	
Nozzle Exit Hole Diameter [μm]	146	
K-factor [−]	2	
Number of holes [Ea]	1	8
Umbrella angle [degree]	N/A	141

mimic the dynamics of the spray through one hole of the MH injector. The SH injector has an orifice along the injector body center axis, as seen in Figure 1C. In contrast, the MH injector has multi-holes off the center axis, as shown in Figure 1D. Nevertheless, due to differences in their internal nozzle structures (Asztalos et al., 2022), the dynamics of sprays exiting the orifice of the SH injector may deviate significantly from that of the MH injector.

2.4 Image and data processing

Figures 1F,G shows the sampled images of the SH and MH injectors. The spray penetration length was defined by 99% of the total spray enveloped area for the SH injector, and the maximum x-location of the perimeter was used for the MH injector. A brief summary of the image processing procedure is as follows:

1. Read the spray images frame by frame.
2. Subtract the background from the raw image.
3. Apply Wiener filter where low pass filters yield a grayscale image that has been degraded by constant power additive noise.
4. Evaluate the threshold using Otsu's method for each image frame to define the threshold applied to all images.
5. Convert grayscale to a binary of black and white images using the threshold.
6. Evaluate spray penetration length.
7. Evaluate the dispersion angle (θ) using two separate definitions:
   a. 60% of maximum spray penetration (60% pen)
   b. 45 times the orifice diameter ($45 \times D_0$).

The 60% pen can capture the far-field spray phenomena well and has been widely adopted in the literature (Tang et al., 2017; Zhang et al., 2017). The alternative definition of $45 \times D_0$ focuses on the dispersion angle near-nozzle region. Therefore, by comparing these two definitions, near- and far-field spray behavior can be highlighted.

A schematic of the MH spray injector orientation, plume index, and the measurement of the actual spray penetration length is shown in Figure 1F,G. The multi-holes are evenly oriented at 45°, and the spray penetration length was measured from the front view. The spray plumes are oriented 19.5° off the plane of the injector, and therefore, the actual

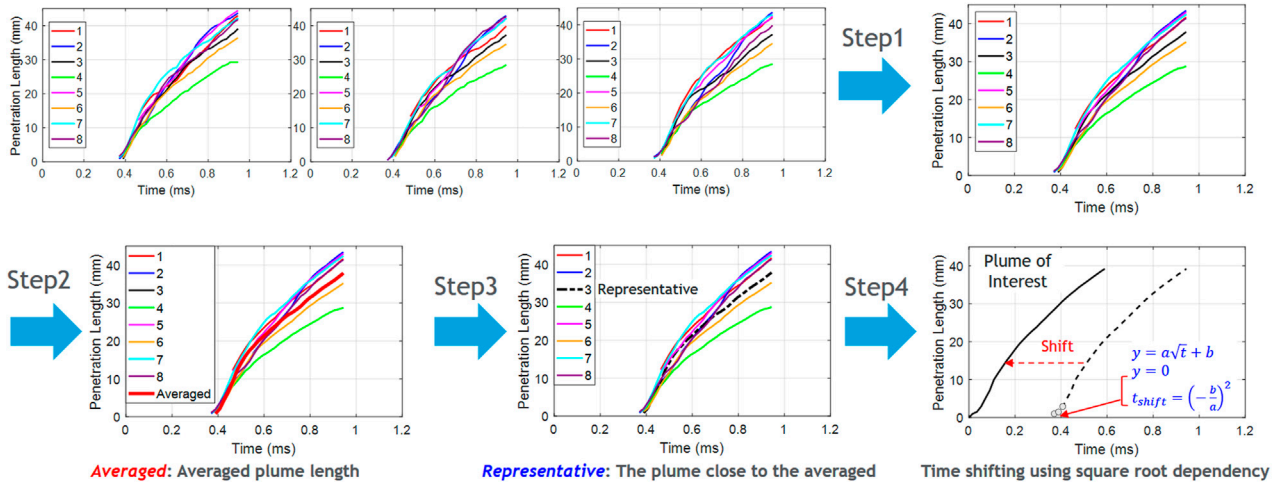

FIGURE 2
Workflow for the determination of SOI and the time origin alignment for spray penetration length of the multi-hole injector.

penetration length (L_p) used in the analysis was calculated based on the visualized penetration length (L) using Eq. 1:

Eq. 1 Correction of the spray penetration length of the MH injector

$$L_p = L/cos(\beta) \tag{1}$$

where β =19.5° is the angle between the actual and measured penetration length axis.

Figure 2 shows a workflow to determine the spray penetration length from the MH injector.

1. The spray penetration length was experimentally measured in three tests, and the mean penetration length of each plume was first evaluated.
2. A plume-averaged penetration length was obtained as denoted by the thick red line.
3. A representative plume index was chosen by comparing the root-mean-square deviation (RMSD) of each plume penetration length with the plume-averaged penetration length.
4. The start-of-injection (SOI) was decided by fitting a square-root function against the first three measurements in the penetration curve to obtain the point of zero penetration.

Following steps 1–4, the spray penetration length from different operating conditions was systematically investigated.

2.5 Test conditions

Table 5 summarizes the experimental test conditions used in this study. The measured experimental data can provide valuable inputs for the engine spray model community because the evaporation effect can be avoided. The nozzle temperature was 15°C, and pure nitrogen (N_2) was used to backfill the vessel.

TABLE 5 Experimental test conditions.

Parameter	Unit	Range		
Fuel	[-]	ULSD		
Ambient temperature (T_a)	[K]	313		
Ambient density (ρ_a)	[kg/m^3]	23	45	65
Injection pressure (P_{inj})	[bar]	500	1,000	1,500
Injection duration (t_{inj})	[ms]	0.5	1.5	

3 Results and discussion

3.1 Spray characterization: Multi-hole ISB injector

3.1.1 Statistical plume-to-plume variation

Unlike the SH injector where the liquid spray is ejected from only one hole, the MH injector includes multiple holes with either symmetrical or asymmetrical hole configurations. Also, the SH injector has the orifice along the vertical axis with the injector body, but the orifices are not along the injector center axis in the MH injector. The different hardware characteristics may affect the in-nozzle flow and needle motion, thereby potentially resulting in different spray penetration behaviors.

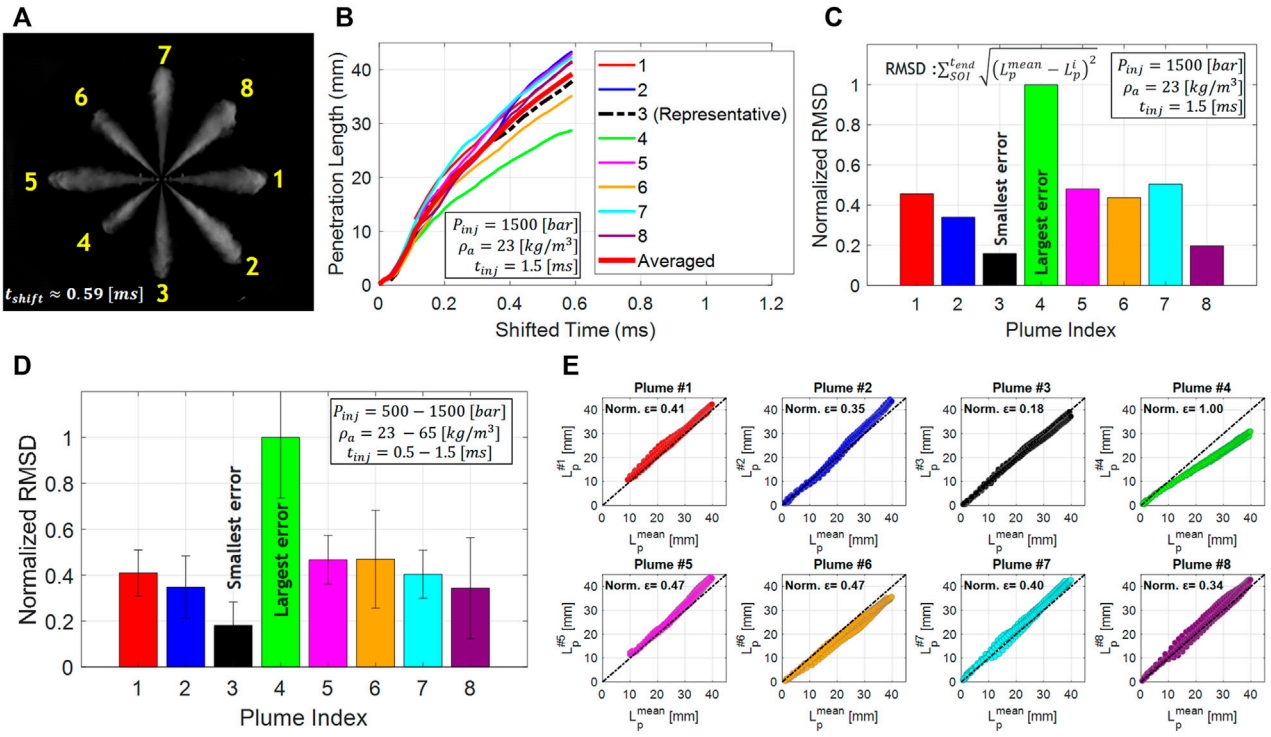

FIGURE 3
(A) Visualized spray penetration at a shifted time t_{shift} = 0.59 [*ms*] and **(B)** comparison of penetration lengths of each plume with the averaged plume (red thick solid). A black-dashed line denotes the representative plume with minimum deviation against the averaged plume. **(C)** Normalized root-mean-square deviation (RMSD) as a function of plume index from the selected operating condition and **(D)** summed RMSD between each plume against the averaged plume. **(E)** Scatter plots of the spray penetration of each plume (L_p^i) against the averaged plume (L_p^{mean}) with normalized deviation (ε), evaluated in wide-ranging operating conditions.

Figure 3A shows the plume index in the MH injector where the starting index is located on the right side, and the index was assigned in a clockwise direction. Figure 3B shows the spray penetration lengths of each plume with different colors, with the averaged plume marked with a thick red line, following the workflow in Figure 2. While the penetration lengths among all eight holes showed similar behavior at the early stage before a shifted time (t_{shift}) of 0.2 ms, deviations occurred afterwards. The most significant deviation was observed near t_{shift} = 0.6 ms, where the plume-to-plume variation differed by up to an approximately 40% relative difference. The RMSD between each plume and the averaged plume (ε) was measured to evaluate the plume-to-plume variation, as shown in Eq. 2:

Eq. 2. The root-mean-square deviation (RMSD) between each plume and the averaged plume

$$\varepsilon_i = \sum_{t=SOI}^{t_{end}} \sqrt{\left(L_p^{mean}(t) - L_p^i(t)\right)^2} \qquad (2)$$

where $L_p(t)$ is the spray penetration length at the time of t. *SOI* and t_{end} are the start-of-injection (SOI) and end-of-measurement, respectively. Superscript i denotes the i^{th} plume and *mean* indicates the averaged plume. Figure 3C shows the RMSD of each plume in the specific condition. A significantly large difference was observed from Plume #4 (green) with the smallest deviation from Plume #3 (black dashed). To further generalize this observation, the RMSD of each plume was summed for all operating conditions and plotted in Figure 3D. As can be seen, the smallest deviation was still observed from Plume #3, while Plume #4 showed the most significant difference with considerable experimental uncertainty. Figure 3E shows the scatter plots of each plume penetration length (L_p^i) compared with the averaged penetration length (L_p^{mean}) collected from all operating conditions with the normalized RMSD value on the title. Plume #4 showed consistently lower RMSD for all conditions considered, while Plume #3 shows a fairly linear correlation with the averaged plume with the smallest RMSD value. Different RMSD behaviors may be associated with hardware characteristics, including hole-to-hole variation in the orifice diameters and internal-nozzle flow patterns caused by eccentric needle motion (Torelli et al., 2017b). This point merits future investigation with X-ray tomography (Moon et al., 2015; Torelli et al., 2018; Sforzo et al., 2022) with internal nozzle flow simulations (Torelli et al., 2017a; Torelli et al., 2017c; Guo H. et al., 2020; Asztalos et al., 2022). To

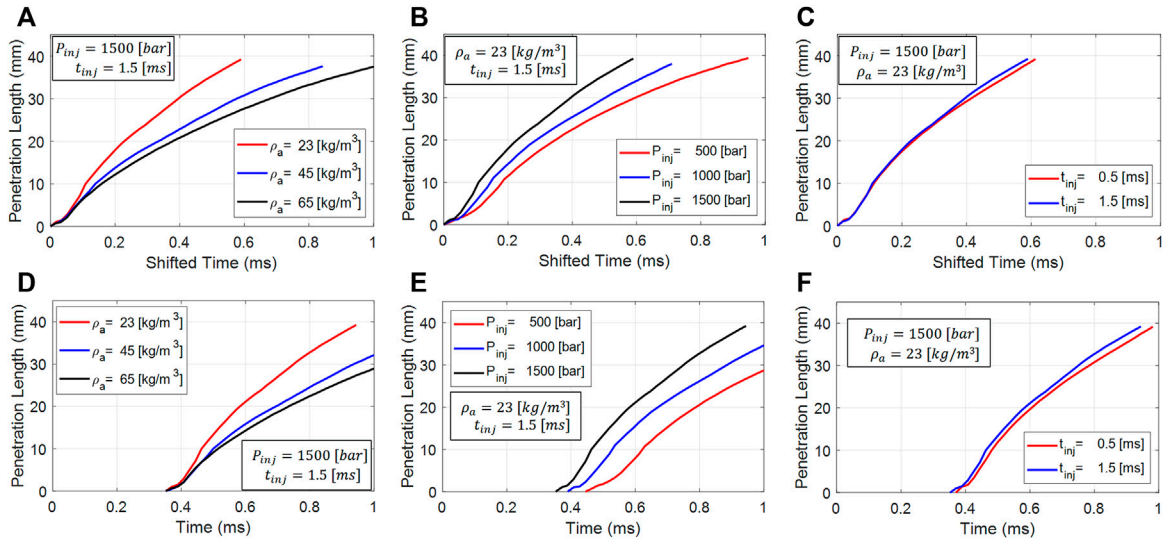

FIGURE 4
The averaged multi-hole spray penetration length as functions of **(A–C)** shifted time and **(D–F)** time, at various operating conditions: effect of, ambient density (ρ_a), fuel injection pressure (P_{inj}), and fuel injection duration (t_{inj}), respectively.

summarize, the statistical analysis demonstrated that an arbitrarily selected plume index (e.g., Plume #4) for the analysis might not represent the averaged plume behavior. Therefore, either the averaged penetration length or a carefully selected plume index should be used to represent the spray characterization of the MH injector.

3.1.2 Effect of operating conditions on the spray penetration

The spray penetration length has been widely studied using the SH injector (Naber and Siebers, 1996; Tang et al., 2017; Zhang et al., 2017), and the following equation has been developed (Naber and Siebers, 1996):

Eq. 3. The empirical equation for the spray penetration length (S)

$$S = \sqrt{\frac{C_v \cdot \sqrt{2C_a}}{a \cdot \tan\left(\frac{\theta}{2}\right)}} \cdot \sqrt{\sqrt{\frac{\left(P_{inj} - P_a\right)}{\rho_a}} \cdot d_o \cdot t} \qquad (3)$$

where C_v and C_a are the velocity and area contraction coefficient of the orifice, respectively, related to the discharge coefficient ($C_d = C_v C_a$). $\theta/2$ is the half of the dispersion angle from the orifice. P_{inj} and P_a are injection and ambient pressure, respectively. ρ_a is the ambient density, d_o is the orifice diameter, and t is the time. a is the constant term assigned to be 0.66 (Naber and Siebers, 1996). Although the above correlation was developed based on the SH injector, it can be used in the MH injector to provide helpful insight for understanding the underlying physics. Following Eq. 3, the faster penetration length may be expected for higher injection pressure and lower ambient density if the dispersion angle is not changed much. It was not possible to accurately determine the dispersion angle for the MH injector in this study due to the front-view camera setup, and thus, only spray penetration is examined.

Figures 4A–C shows the effects of (A) ambient density, (B) injection pressure, and (C) injection duration on the spray penetration length at wide ranges of engine-relevant operating conditions. The SOI is obtained following the procedure in Figure 2, and the averaged plume penetration lengths from the MH ISB injector are plotted as functions of the shifted time. Figure 4A shows the spray penetration length with different ambient density conditions at a fixed injection pressure of 1,500 bar and an injection duration of 1.5 ms. The higher penetration length was observed at lower ambient density conditions, as inferred by Eq. 3. The effects of injection pressure on the spray penetration length were also found following the general trend expressed by Eq. 3, as seen in Figure 4B, indicating that the governing physics of the spray penetration of the MH injector is similar to the SH injector. On the other hand, the injection duration from 0.5 to 1.5 ms did not show a noticeable difference, as seen in Figure 4C.

While the general spray penetration lengths showed similar trends between the SH and MH injectors, the different nozzle configurations may have caused a non-negligible impact on the spray penetration, as seen in Figures 1C,D. In order to investigate this point, the spray penetration length was re-plotted against the original time without the time shift in Figures 4D–F. At an injection pressure of 1,500 bar, the spray penetration curves of

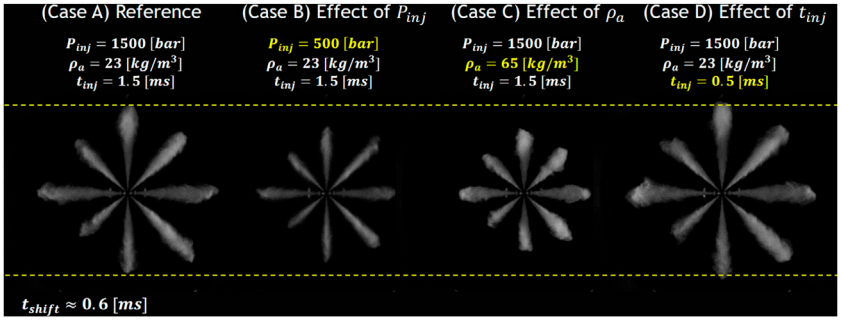

FIGURE 5
Visualization of the multi-hole spray penetration length observed from the front view in various operating conditions.

different ambient densities and injection durations showed a similar SOI of $t = 3.7$ ms. However, the spray penetration in lower injection pressure conditions showed delayed SOIs corresponding to 0.40 and 0.46 ms for 1,000 and 500 bar, respectively. This indicates that for the lower injection pressure conditions, the rate of needle lift or sac pressure rise may be slower, resulting in a delayed SOI (i.e., longer hydraulic delay) and a slower ramp-up during the initial rate-of-injection (ROI) profile, as observed in Dong et al. (2016) and Jin et al. (2020). Overall, the effects of the ambient density, injection pressure, and injection duration of the MH spray penetrations can be explained based on the empirical equation as seen in Eq. 3, developed based on the SH injector.

Figure 5A–D shows the 2D snapshot from the bottom side view for various operating conditions to highlight the effects of the injection pressure (Case B), ambient density (Case C), and injection duration (Case D). All operating conditions showed apparent plume-to-plume variations, as reported in Figure 3C, where Plume #4 has a noticeably shorter spray penetration length than others, and Plume #3 exhibits the nominal spray penetration behavior compared with other plumes. These images confirm that an arbitrarily selected plume index (e.g., Plume #4) may not represent the averaged plume behavior. Interestingly, a similar asymmetric spray penetration trend was observed in all cases, indicating that it must be associated with hardware characteristics, e.g., different orifice diameters or in-nozzle flow characteristics.

In parallel work, the same series of the injector with a different part number was scanned using a high-resolution X-ray (Sforzo et al., 2022) to generate a realistic geometry, and applied to in-nozzle flow CFD simulations (Asztalos et al., 2022). With a gasoline-like fuel, a similar plume-to-plume variation was observed in particular nozzles [e.g., Orifices #3 and #4 as denoted in Asztalos et al., 2022], indicating that the observation is not likely due to malfunctioning of the injector. In addition, we investigated other MH injectors (e.g., heavy-duty ISX) in our previous work and observed similar plume-to-plume variations in the mass flow ROI. Variabilities exceeded what was expected from the variation in geometry (i.e., hole area) alone and were strongly correlated with the eccentric needle motion (i.e., wobble) inside the injector.

3.1.3 Evaluation of an arbitrary plume index

As shown in Figure 5 and in the spray penetration statistics in Figure 3C–E, the plume-to-plume variation of the medium-duty ISB injector was noticeably different. A nominal trend was captured using Plume #3, while a large difference was evident in Plume #4. To further verify the importance of the plume index selection, Figure 6 shows the spray penetration length of averaged plume penetration compared with differently selected plumes of interest for selected operating conditions. Note that the penetration of Plumes #1 and #5 started more slowly than other plumes because of the object reflected in the visualized image at the early stages. These points were excluded when the averaged penetration length was calculated. As expected, a significantly deviated trend was obtained from Plume #4, where the largest difference was observed, as seen in Figure 3C–E. The comparisons of the spray penetrations from each hole show clear plume-to-plume variation, further demonstrating that arbitrarily selected plumes can mislead the spray characterization. To be specific, if Plume #8 or #7 had been selected as a target plume, the relative injection pressure effects could not have been captured. Interestingly, Plume #3 showed a statistically nominal plume that followed the averaged plume behavior. Thus, once plume-to-plume variation is systematically investigated, a specific plume index can be selected and used to characterize the spray penetration behavior in the MH injector.

3.2 Spray characterization: Single-hole ISB injector

In this section, an SH medium-duty ISB injector is systematically described. While only the spray penetration

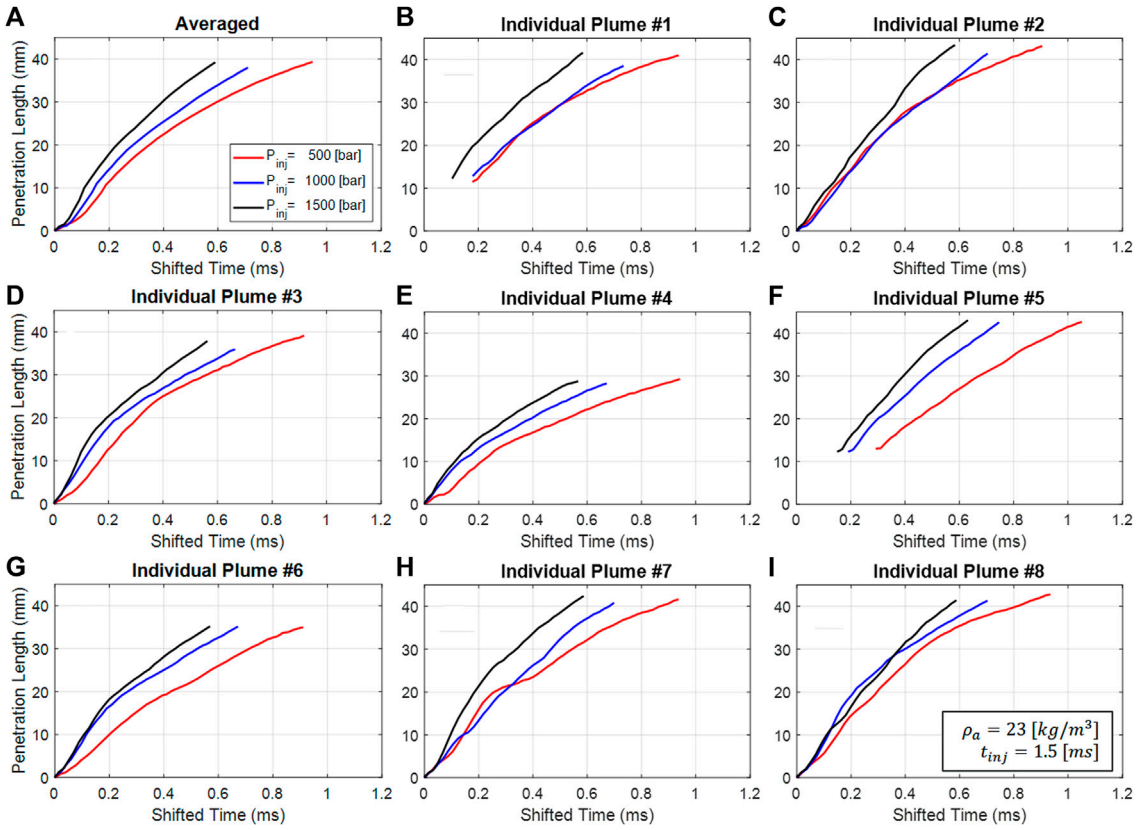

FIGURE 6
Spray penetration length of the multi-hole injector with different definitions of plumes of interest: **(A)** averaged plume behavior (solid line), **(B–I)** Plumes #1–8, at an ambient density of 23 kg/m^3 and injection duration of 1.5 ms.

length was measured for the MH injector, both dispersion angle and spray penetration length were measured for the SH injector. Also, two different definitions of the dispersion angle were evaluated to elucidate their difference.

Figure 7A,B shows the determination of the dispersion angle (θ) of the SH injector with two different definitions: 1) 60% of the maximum spray penetration length (60% pen), and 2) 45 times the orifice diameter (45 $\times D_0$), as introduced in Figure 1E. The steady-state dispersion angle was first determined from the three repetitions, as seen in Figure 7A,B, and the comparisons between the two definitions are shown in Figure 7C. The 60% pen showed a larger dispersion angle but smaller experimental uncertainty (standard deviation) than 45 $\times D_0$. At the early stage, both definitions showed very similar dispersion angles until 0.15 ms, and then started to deviate with a maximum difference of 42% at 0.5 ms. Figure 7D shows the 2D instantaneous side views from the two definitions at the selected points (A and B), as denoted in Figure 7C. As can be seen, while the two definitions showed very similar dispersion angles at the early stage, the 60% pen showed a larger dispersion angle compared to 45 $\times D_0$ at a later stage due to the broader spray boundary (green color) at the far field. The measured dispersion angle data using the two definitions can be useful validation targets for engine spray modeling to capture near-to far-field spray dispersion behaviors.

3.3 Comparison between single- and multi-hole ISB injectors

Figure 8 compares spray penetration lengths between the medium-duty SH and MH injectors. As seen in Figure 8A, for the same operating condition, the SH injector (black circle) showed faster spray penetration than the MH injector (red triangle). In particular, the MH injector showed a smaller initial slope (dS/dt) than the SH injector, indicating that the MH injector exhibits a slower rate of effective nozzle flow area increase than the SH injector, as reported in several studies (Dong et al., 2017; Jin et al., 2020). Although the initial slope is quite different between the SH and MH injectors, the spray penetrations at the later stage show a linearly correlated trend. To confirm this point, the scatter plot of the spray penetration lengths is presented in Figure 8B. By truncating the initial moments ($t < 0.01\,ms$), the spray penetrations of the SH and MH injectors showed a strong

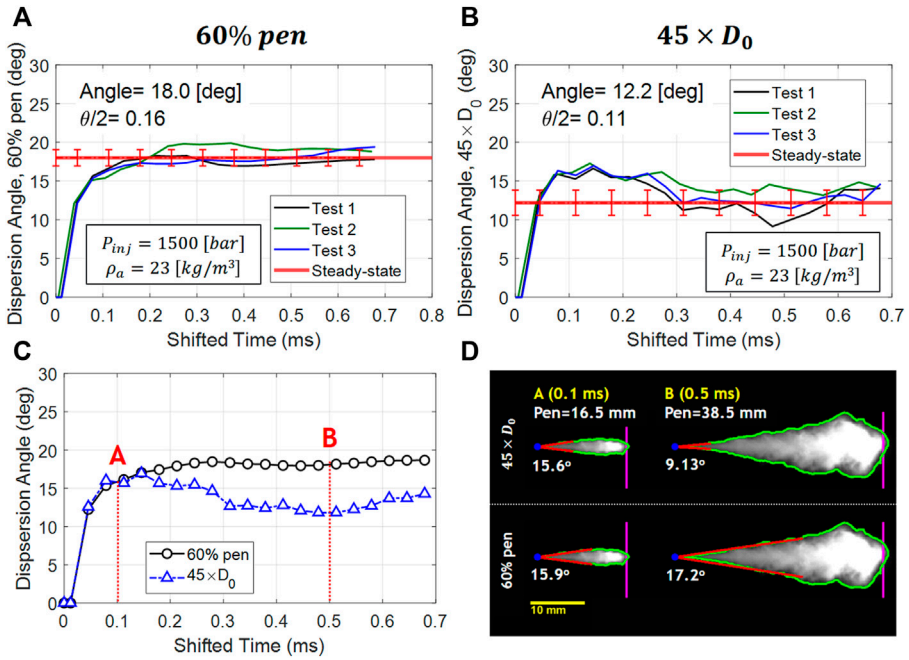

FIGURE 7
Dispersion angle of the single-hole injector from different definitions: **(A)** 60% of maximum penetration (60% pen) and **(B)** 45 times the orifice diameter (45 × D_0), with averaged dispersion angle at a steady state with measurement uncertainty. **(C)** Transient averaged dispersion angles from two separate definitions at points A and B **(D)** Instantaneous snapshots of the 2D side view from the selected time instances marked in **(C)**.

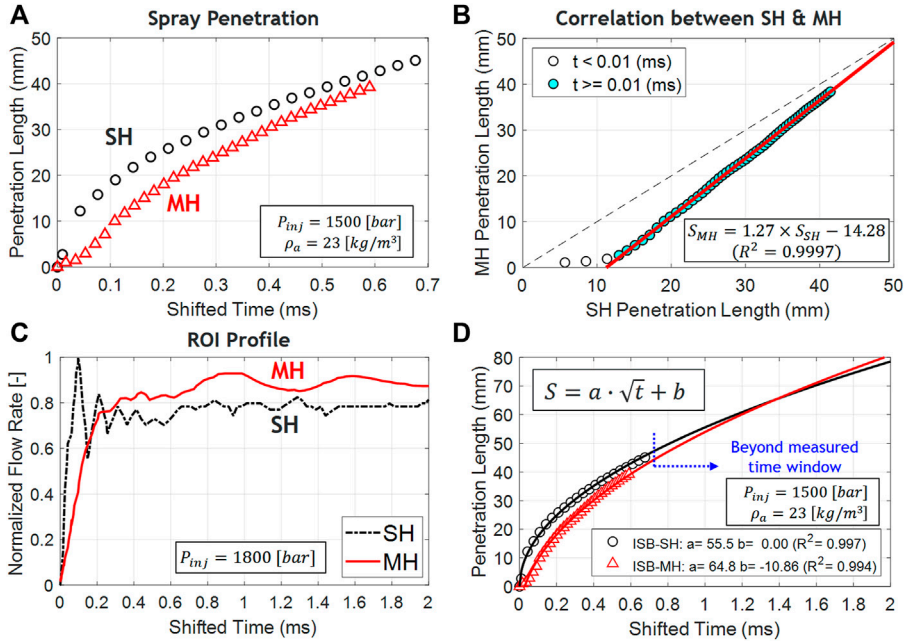

FIGURE 8
(A) Comparison of spray penetration between medium-duty SH (black) and MH (red) injectors. **(B)** Scatter plot of the penetration length of the SH and MH injectors with a linear correlation curve. **(C)** Normalized rate-of-injection (ROI) profiles using the SH and MH injectors at an injection pressure of 1,800 bar. **(D)** Spray penetration correlation obtained for the SH and MH injectors.

linear correlation with a high R^2 value of 0.9997. This indicates that although the spray penetration length is affected by the sac pressure and the effective nozzle flow area development at the initial stage, it will be governed by the in-cylinder environmental condition at the later stage. To confirm this point, the ROI profiles measured from the ISB SH and MH injectors are shown in Figure 8C. As the measured flow rate of the MH injector included all eight holes, the single-hole equivalent flow rate results are plotted. Similar to Figure 8A, the SH injector showed a faster ramp-up compared to the MH injector, where the early stage of ramp-in was associated with the in-nozzle transient flow, sac pressure, and orifice hardware characteristics. A similar observation was made in several other studies (Jung et al., 2015; Dong et al., 2016; Jin et al., 2020), and Dong et al. (2016) calculated the sac pressure from the injection rate curves and found that the sac pressure of the SH injector increased much faster than that of the MH injector due to the effective nozzle flow area. Interestingly, while the MH injector showed a slower ramp-up, it started to exceed the SH injector after $t_{shift} = 0.2\,ms$ with a 15% higher flow rate at a steady-state period. This indicates that the discharge coefficient of the MH injector is higher than the SH injector, as observed from the previous work using ECN SH A and 3-hole B injectors (Jung et al., 2015). Similarly, the experimental spray data of the MH injector showed a slower ramp-up at the early stage but became comparable with the SH injector at a later stage. Although the MH injector did not exceed the SH injector during this observation time window ($t_{shift} < 0.7\,ms$), the MH spray is likely to have exceeded the SH spray at a later time. To confirm this point, the spray penetration curves from SH and MH injectors were fitted into the square-root function. Figure 8D shows the original raw data with symbols, the fitted equation with solid lines, and the coefficients in the legend. The fitted curve shows good agreement with the original data within the observation window. Then the MH spray started to be comparable with the SH spray and finally exceeded the SH spray after t_{shift} = 1.4 ms. The deviation in the crossover time between ROI and spray penetration data is likely due to the different injection pressure and other boundary conditions. The spray and ROI data revealed that while the SH injector showed a faster ramp-up than the MH injector, the MH injector became comparable with the SH injector, and then started to exceed the SH injector at a later time with both SH and MH spray data following the well-known square-root dependency (Naber and Siebers, 1996).

3.4 Comparison between medium-(ISB) and heavy-(ISX) duty single-hole injectors

The key injector specifications of the heavy-duty (ISX) and medium-duty (ISB) injectors are summarized in Table 6. The ISB injector has a smaller nozzle exit hole diameter and a slightly larger K-factor than the ISX injector. The discharge coefficient was not available for the ISB SH injector, while that of the ISX SH injector had a value of 0.94 (Tang et al., 2017). Both injectors consisted of a solenoid-driven, hydraulically lifted main needle, and the hole was along the central axis of the injector, as seen in Figure 1B.

TABLE 6 Injector specification of the heavy- and medium-duty single-hole injectors.

	ISX SH injector (heavy-duty)	ISB SH injector (medium-duty)
Nozzle exit hole diameter [μm]	176	146
K-factor [−]	1.8	2
Discharge coefficient (C_d) (Re = 12,000)	0.94	N/A
Area coefficient (C_a)	0.95	N/A

Figure 9A compares dispersion angles with the 60% pen definition between ISX and ISB injectors. The two injectors showed very similar dispersion angle results at the steady state, and the relative difference was only 1.7%. Figure 9B shows the measured dispersion angles from the ISX and ISB injectors compared with the existing measurements with different orifice diameters from the previous studies (Naber and Siebers, 1996). The correlation equation was also plotted with 1-deg bounds. The measured values from ISB and ISX injectors show good alignment with other measurements and correlation within 1-deg bounds. Figure 9C shows the spray penetration length between ISB and ISX SH injectors, where the symbols denote the experimental measurements while the solid lines are the fitted equation with a square-root function. Both injectors showed good agreements with the empirical equations with high R^2 values (>0.99), indicating that both injectors follow a square-root dependency due to the air entrainment into the spray envelope, similar to prior work (Naber and Siebers, 1996; Tang et al., 2017; Tang, 2018). The ISX injector showed faster penetration than the ISB injector as spray penetration length is proportional to the orifice diameter, as expressed in Eq. 3, under the same operating conditions (e.g., P_{inj}, P_a, ρ_a) and similar dispersion angle (θ/2), as seen in Figure 9. However, it is noted that the spray penetration is also affected by other factors, including velocity (C_v) and area (C_a) coefficients through the discharge coefficient (C_d). The discharge coefficient can provide useful information regarding the actual mass flow rate compared with the theoretical flow rate, considering the area contraction, cavitation, and so on. Unfortunately, an accurate discharge coefficient measurement of the ISB injector was not available at that time, which limits further quantitative examination.

To further investigate the different spray penetration behaviors between the ISB and ISX injectors, the scatter plots of the two injectors are shown in Figure 9D. As can be seen, these two injectors show a linear trend at the early stage until t <

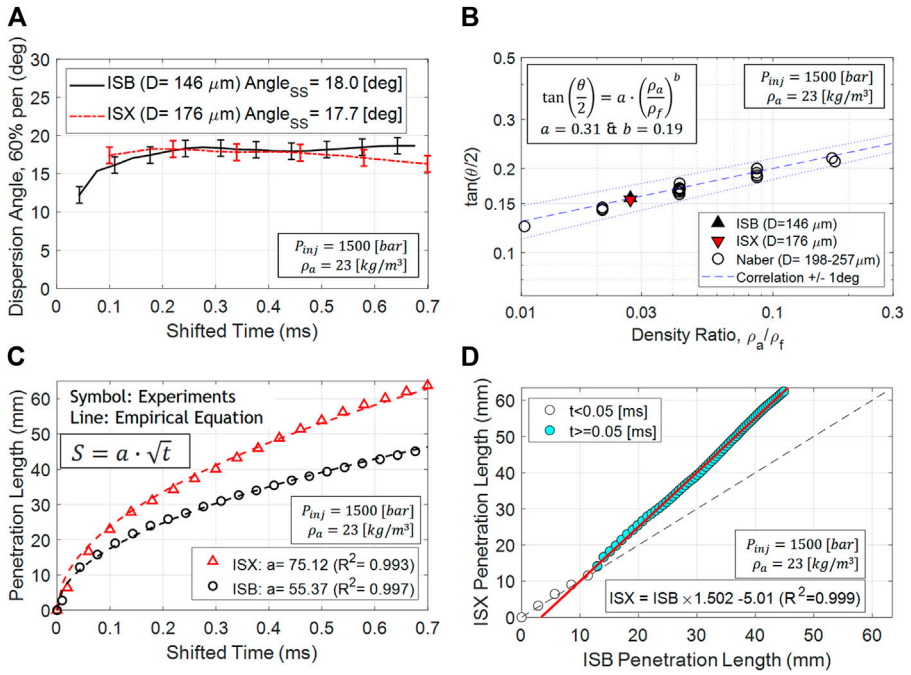

FIGURE 9
(A) Comparison in dispersion angle (60% pen) between the ISX and ISB injectors where subscript SS indicates quasi-steady state. **(B)** Comparison with previous studies (Naber and Siebers, 1996) where ρ_f is the fuel density. **(C)** Comparison of the spray penetration lengths between the ISB and ISX injectors (symbols) with fitted square-root correlations (dashed lines). **(D)** Scatter plot of the spray penetration length of the ISX and ISB injectors with a linear correlation curve. The experimental data measured at an ambient density of 23 kg/m^3 and an injection pressure of 1,500 bar was used.

0.05 ms because both injectors have a single hole along the injector axis. As such, the internal flow characteristic is quite similar. After the early stage, the ISX injector started to penetrate faster than the ISB injector due to different air entrainment effects caused by a larger injector nozzle diameter (176 μm for ISX vs. 146 μm for ISB).

4 Summary

Experimental diesel spray characterization was performed in an optically accessible, constant-volume combustion chamber through Cummins medium-duty ISB injectors. The purpose of this study was to 1) measure the spray penetration length of the MH injector, 2) characterize the plume-to-plume variation, and 3) compare the penetration length of the MH injector with the corresponding SH injector. The dispersion angle was measured for the SH injector with two separate definitions to distinguish the near-nozzle and far-field characteristics. The spray penetration length and dispersion angle from the ISB SH injector was further compared with that of a heavy-duty ISX SH injector. The measured experimental data and empirical correlations obtained can be used as valuable inputs to develop and improve spray models. Our major findings follow.

The MH injector showed plume-to-plume variation in the spray penetration length. The hole-averaged penetration length and each spray plume were systematically measured. A significantly large deviation was measured from the specific hole (Plume #4) against the averaged behavior, while a good correlation was observed from the other hole (Plume #3). This indicates that selecting an arbitrary plume index to characterize the spray penetration length may not accurately represent the averaged plume behavior. The spray penetration length of the MH injector showed a similar trend to the empirical spray penetration equation developed from the SH injector. Slower penetration behavior was observed at a lower injection pressure (500 bar) compared to higher injection pressures (1,000–1,500 bar), and higher ambient density (45–65 kg/m^3) compared to a lower ambient density (23 kg/m^3). In contrast, different injection duration times (0.5–1.5 ms) did not show a noticeable difference.

For the SH injector, two different definitions of the dispersion angle were used to quantitatively assess the spray behavior: 1) 60% of the maximum penetration length (60% pen) and 2) 45 times the orifice diameter (45 × D_0). Both showed similar transient behavior at the early stage but 60% pen started to show a larger dispersion angle than the 45 × D_0 downstream due to the broader spray boundary. While the dispersion angle with 60% pen from the ISX and ISB injectors showed a similar

trend, the ISX injector showed a faster penetration than the ISB injector. The two injectors showed a similar penetration development at the early stage, while the ISX injector started to penetrate faster than the ISB injector by a factor of 1.5 due to the air entrainment effect caused by a larger injector diameter later (176 vs. 146 μm).

The spray penetration of the MH injector showed a slower initial ramp-up than the SH injector. The measured ROI profile showed a similar pattern, indicating that the slower penetration of the MH injector is likely associated with the slower development of the sac pressure and the effective nozzle flow area. While the MH spray showed slower penetration and volumetric flow rate than the SH injector at the early stage, the MH spray started to be comparable with the SH spray, and finally, exceeded it at a later stage. This indicates that the discharge coefficients of the MH injector may be larger than the SH injector in a quasi-steady-state period. Finally, the square-root correlations were developed to model the spray penetration of the SH and MH injectors, showing good agreement with the measured data.

Data availability statement

The datasets presented in this article are not readily available because approval from all author affiliations is needed on a case-by-case bases before access can be granted. Requests to access the datasets should be directed to ji-woong.park@aramcoamericas.com.

Author contributions

This work was a joint project collaboration among three organizations: Michigan Technological University (MTU), Cummins, and Aramco Americas: Aramco Research Center—Detroit. The spray measurements were performed by the MTU group. Aramco and Cummins provided guidance and coordination throughout the project. J-WP has performed the post-processing of the test data and documented the analysis. J-WP's academic research is supervised by SS. This manuscript was prepared and revised based on inputs from the authors of all three organizations.

Acknowledgments

This work is part of a larger effort known as the U.S.-China CERC-Truck Collaborative Knowledge Consortium. The spray tests were conducted in MTU's spray lab. Cummins Fuel Systems designed and manufactured the SH injector for the project and provided both SH and MH ISB injectors for the study.

Conflict of interest

Authors J-WP, TT, YP, and YZ were employed by Aramco Americas: Aramco Research Center–Detroit, Novi, MI, United States and Authors FT, RG, and DL were employed by Cummins Inc., Columbus, IN, United States.

The remaining authors declare that the research was conducted in the absence of any commercial or financial relationships that could be construed as a potential conflict of interest.

Publisher's note

References

Arcoumanis, C., Flora, H., Gavaises, M., and Badami, M. (2000). Cavitation in real-size multi-hole diesel injector nozzles. SAE Technical Paper. doi:10.4271/2000-01-1249

Asztalos, K. J., Torelli, R., Pei, Y., Zhang, Y., Tao, F., Garg, R., et al. (2022). "Application of modal decomposition techniques to characterize the internal nozzle flow of a medium-duty diesel injector operating with gasoline-like fuels," in ASME 2022 internal combustion engine div. fall technical conference, ICEF, October 16–19, 2022, Indianapolis, IN, United States, 1–12.

AVL FIRE (2013). *AVL Fire Version 2013 User Manual* .

Battistoni, M., Som, S., and Powell, C. F. (2019). Highly resolved eulerian simulations of fuel spray transients in single- and multi-hole injectors : Nozzle flow and near-exit dynamics. *Fuel* 251, 709–729. doi:10.1016/j.fuel.2019.04.076

Benajes, J., Payri, R., Bardi, M., and Martí-Aldaraví, P. (2013). Experimental characterization of diesel ignition and lift-off length using a single-hole ECN injector. *Appl. Therm. Eng.* 58, 554–563. doi:10.1016/j.applthermaleng.2013.04.044

Chen, B., Feng, L., Wang, Y., Ma, T., Liu, H., Geng, C., et al. (2019). Spray and flame characteristics of wall-impinging diesel fuel spray at different wall temperatures and ambient pressures in a constant volume combustion vessel. *Fuel* 235, 416–425. doi:10.1016/j.fuel.2018.07.154

Choi, M., and Park, S. (2022). Optimization of multiple-stage fuel injection and optical analysis of the combustion process in a heavy-duty diesel engine. *Fuel Process. Technol.* 228, 107137. doi:10.1016/j.fuproc.2021.107137

D'Ambrosio, S., and Ferrari, A. (2015). Effects of exhaust gas recirculation in diesel engines featuring late PCCI type combustion strategies. *Energy Convers. Manag.* 105, 1269–1280. doi:10.1016/J.ENCONMAN.2015.08.001

Dong, P. B., Nishida, K., Inaba, T., and Ogata, Y. (2016). Characterization of internal flow and spray behaviors of hole-type nozzle under tiny and normal injection quantity conditions for diesel engine. *SAE Int. J. Fuels Lubr.* 9, 125–137. doi:10.4271/2016-01-0862

Dong, P., Nishida, K., and Ogata, Y. (2017). Characterization of multi-hole nozzle sprays and internal flow for different nozzle hole lengths in direct-injection diesel

engines. *Proc. Institution Mech. Eng. Part D J. Automob. Eng.* 231, 500–515. doi:10.1177/0954407016653890

Eagle, W. E., Malbec, L. M., and Musculus, M. P. B. (2016). Measurements of liquid length, vapor penetration, ignition delay, and flame lift-off length for the engine combustion network 'spray B' in a 2.34 L heavy-duty optical diesel engine. *SAE Int. J. Engines* 9, 910–931. doi:10.4271/2016-01-0743

Engine Combustion Network (ECN) (2022). The ECN is an international collaboration among experimental and computational researchers in engine combustion. Available at: https://ecn.sandia.gov/ (Accessed January, 2022).

Garcia, E. (2021). Strategies for improving efficiency and emissions in heavy-duty diesel engines. Thesis. University of Michigan.

García-Oliver, J. M., Novella, R., Pastor, J. M., and Pachano, L. (2020). Computational study of ECN spray A and spray D combustion at different ambient temperature conditions. *Transp. Eng.* 2, 100027. doi:10.1016/j.treng.2020.100027

Guo, Z., He, X., Pei, Y., Chang, C-T., Wang, P., Sun, X., et al. (2020). Optimization of piston bowl geometry for a low emission heavy-duty diesel engine. SAE Technical Paper. doi:10.4271/2020-01-2056

Guo, H., Torelli, R., Rodriguez, A. B., Tekawade, A., Sforzo, B., Powell, C., et al. (2020). Internal nozzle flow simulations of the ECN spray. *SAE J Adv Curr Prac Mobil.* 2 (4), 2229–2240. doi:10.4271/2020-01-1154

Huang, W., Moon, S., Gao, Y., Li, Z., and Wang, J. (2017). Eccentric needle motion effect on near-nozzle dynamics of diesel spray. *Fuel* 206, 409–419. doi:10.1016/j.fuel.2017.06.012

International Energy Agency (2021). World energy outlook 2021. Available at: https://www.iea.org/reports/world-energy-outlook-2021 (Accessed January, 2022).

Jin, Y., Kim, J., Kakami, S., Nishida, K., Ogata, Y., and Luo, H. (2020). Comparison of diesel spray with small injection amount between single-hole and multi-hole injectors: Results under same rail pressure and similar injection rate. *Int. Commun. Heat Mass Transf.* 118, 104862. doi:10.1016/j.icheatmasstransfer.2020.104862

Jung, Y., Manin, J., Skeen, S., and Pickett, L. M. (2015). Measurement of liquid and vapor penetration of diesel sprays with a variation in spreading angle. SAE Technical Paper. doi:10.4271/2015-01-0946

Kennaird, D. A., Crua, C., Lacoste, J., Heikal, M. R., Gold, M. R., and Jackson, N. S. (2002). In-cylinder penetration and break-up of diesel sprays using a common-rail injection system. SAE Technical Paper. doi:10.4271/2002-01-1626

Kook, S., and Pickett, L. M. (2012). Liquid length and vapor penetration of conventional, fischer-tropsch, coal-derived, and surrogate fuel sprays at high-temperature and high-pressure ambient conditions. *Fuel* 93, 539–548. doi:10.1016/j.fuel.2011.10.004

Liu, L., Mei, Q., and Jia, W. (2022). A flexible diesel spray model for advanced injection strategy. *Fuel* 314, 122784. doi:10.1016/j.fuel.2021.122784

Moon, S., Gao, Y., Park, S., Wang, J., Kurimoto, N., and Nishijima, Y. (2015). Effect of the number and position of nozzle holes on in- and near-nozzle dynamic characteristics of diesel injection. *Fuel* 150, 112–122. doi:10.1016/j.fuel.2015.01.097

Naber, J. D., and Siebers, D. L. (1996). Effects of gas density and vaporization on penetration and dispersion of diesel sprays. SAE Technical Paper. doi:10.4271/960034

Nesbitt, J. E., Naber, J. D., Lee, S., Kurtz, E., Ge, H., and Hills, F. (2011). "Investigation of vaporizing diesel liquid spray plume to plume penetration variations," in ILASS americas, 23rd annual conference on liquid atomization and spray systems, Ventura, CA, May 2011.

Pastor, J. V., Payri, R., Garcia-Oliver, J. M., and Nerva, J. G. (2012). Schlieren measurements of the ECN-spray A penetration under inert and reacting conditions. SAE Technical Paper. doi:10.4271/2012-01-0456

Pastor, J. V., Garcia-Oliver, J. M., Garcia, A., and Morales López, A. (2018). An experimental investigation on spray mixing and combustion characteristics for spray C/D nozzles in a constant pressure vessel. SAE Technical Paper. doi:10.4271/2018-01-1783

Payri, F., Payri, R., Bardi, M., and Carreres, M. (2014). Engine combustion network: influence of the gas properties on the spray penetration and spreading angle. *Exp. Therm. Fluid Sci.* 53, 236–243. doi:10.1016/j.expthermflusci.2013.12.014

Payri, R., Salvador, F. J., Manin, J., and Viera, A. (2016). Diesel ignition delay and lift-off length through different methodologies using a multi-hole injector. *Appl. Energy* 162, 541–550. doi:10.1016/j.apenergy.2015.10.118

Payri, R., Gimeno, J., Cuisano, J., and Arco, J. (2016). Hydraulic characterization of diesel engine single-hole injectors. *Fuel* 180, 357–366. doi:10.1016/j.fuel.2016.03.083

Payri, R., Gimeno, J., Cardona, S., and Ayyapureddi, S. (2019). Experimental study of the influence of the fuel and boundary conditions over the soot formation in multi-hole diesel injectors using high-speed color diffused back-illumination technique. *Appl. Therm. Eng.* 158, 113746. doi:10.1016/j.applthermaleng.2019.113746

Pei, Y., Davis, M. J., Pickett, L. M., and Som, S. (2015). Engine combustion network (ECN): global sensitivity analysis of spray A for different combustion vessels. *Combust. Flame* 162, 2337–2347. doi:10.1016/j.combustflame.2015.01.024

Pickett, L. M., Manin, J., Payri, R., Bardi, M., and Gimeno, J. (2013). Transient rate of injection effects on spray development. SAE Technical Paper. doi:10.4271/2013-24-0001

Pomraning, E., Richards, K., and Senecal, P. K. (2014). Modeling turbulent combustion using a RANS model, detailed chemistry, and adaptive mesh refinement. SAE Technical Paper. doi:10.4271/2014-01-1116

Sellnau, M., Foster, M., Moore, W., Sinnamon, J., Hoyer, K., and Klemm, W. (2019). Pathway to 50% brake thermal efficiency using gasoline direct injection compression ignition. SAE Technical Paper. doi:10.4271/2019-01-1154

Senecal, P. K., Pomraning, E., Richards, K. J., Briggs, T. E., Choi, C. Y., McDavid, R. M., et al. (2003). Multi-dimensional modeling of direct-injection diesel spray liquid length and flame lift-off length using CFD and parallel detailed chemistry. SAE Technical Paper. doi:10.4271/2003-01-1043

Sforzo, B. A., Tekawade, A., Kastengren, A. L., Fezzaa, K., Ilavsky, J., Powell, C. F., et al. (2022). X-ray characterization of real fuel sprays for gasoline direct injection. *J. Energy Resour. Technol.* 144, 1–7. doi:10.1115/1.4050979

Siebers, D., and Higgins, B. (2001). Flame lift-off on direct-injection diesel sprays under quiescent conditions. SAE Technical Paper. doi:10.4271/2001-01-0530

Siebers, D. L. (1998). Liquid-phase fuel penetration in diesel sprays. SAE Technical Paper. doi:10.4271/980809

Siebers, D. L. (1999). Scaling liquid-phase fuel penetration in diesel sprays based on mixing-limited vaporization. SAE Technical Paper. doi:10.4271/1999-01-0528

Subramanian, S., Rathinam, B., Lalvani, J. I. J., and Annamalai, K. (2016). Piston bowl optimization for single cylinder diesel engine using CFD. SAE Technical Paper. doi:10.4271/2016-28-0107

Tang, M., Zhao, L., Lee, S. Y., and Naber, J. (2016). Effect of combustion on diesel spray penetrations in relation to vaporizing, non-reacting sprays. SAE Technical Paper. doi:10.4271/2016-01-2201

Tang, M., Zhang, J., Menucci, T., Schmidt, H., Naber, J., Lee, S. Y., et al. (2017). "Experimental spray ignition and soot forming characteristics of high reactivity gasoline and diesel fuel in a heavy-duty single-hole injector," in ILASS americas 29th annual conference on liquid atomization and spray systems, Atlanta, GA, April 2017.

Tang, M., Pei, Y., Zhang, Y., Tzanetakis, T., Traver, M., Cleary, D., et al. (2018). Development of a transient spray cone angle correlation for CFD simulations at diesel engine conditions. SAE Technical Papeer. doi:10.4271/2018-01-0304

Tang, M. (2018). Spray and combustion studies of high reactivity gasoline in comparison to diesel under advanced compression ignition engine conditions. PhD dissertation. Michigan Tech.

Tennison, P. J., Georjon, T. L., Farrell, P. V., and Reitz, R. D. (1998). An experimental and numerical study of sprays from a common rail injection system for use in an HSDI diesel engine. SAE Technical Paper. doi:10.4271/980810

Torelli, R., Som, S., Pei, Y., Zhang, Y., Voice, A., Traver, M., et al. (2017). Comparison of in-nozzle flow characteristics of naphtha and N-dodecane fuels. SAE Technical Paper. doi:10.4271/2017-01-0853

Torelli, R., Som, S., Pei, Y., Zhang, Y., and Traver, M. (2017). Influence of fuel properties on internal nozzle flow development in a multi-hole diesel injector. *Fuel* 204, 171–184. doi:10.1016/j.fuel.2017.04.123

Torelli, R., Som, S., Pei, Y., Zhang, Y., and Traver, M. (2017). "Internal nozzle flow simulations of gasoline-like fuels under diesel operating conditions," in ILASS americas 29th annual conference on liquid atomization and spray systems, Atlanta, GA, April 2017.

Torelli, R., Matusik, K. E., Nelli, K. C., Kastengren, A. L., Fezzaa, K., Powell, C. F., et al. (2018). Evaluation of shot-to-shot in-nozzle flow variations in a heavy-duty diesel injector using real nozzle geometry. *SAE Int. J. Fuels Lubr.* 11, 295. doi:10.4271/2018-01-0303

Tzanetakis, T., Voice, A. K., and Traver, M. (2021). Accurately simulating the performance of gasoline-like fuels in 1-D hydraulic injection system models operating at high pressures. SAE Technical Paper. doi:10.4271/2021-01-0389

Tzanetakis, T., Johnson, J., Schmidt, H., Atkinson, W., and Naber, J. (2022). Non-reacting spray characteristics of gasoline and diesel with a heavy-duty single-hole injector. *Front. Mech. Eng.* 8, 1–16. doi:10.3389/fmech.2022.887657

U.S. Energy Information Administration (2021). *Annual energy outlook 2021*. Available at: https://www.eia.gov/outlooks/aeo/ (Accessed January, 2022).

Yao, T., Pei, Y., Zhong, B. J., Som, S., Lu, T., and Luo, K. H. (2017). A compact skeletal mechanism for *n*-dodecane with optimized semi-global low-temperature chemistry for diesel engine simulations. *Fuel* 191, 339–349. doi:10.1016/j.fuel.2016.11.083

Yasutomi, K., Hwang, J., Pickett, L. M., Sforzo, B., Matusik, K., and Powell, C. F. (2020). Transient internal nozzle flow in transparent multi-hole diesel injector. SAE Technical Paper. doi:10.4271/2020-01-0830

Yi, W., Liu, H., Feng, L., Wang, Y., Cui, Y., Liu, W., et al. (2021). Multiple optical diagnostics on effects of fuel properties on spray flames under oxygen-enriched conditions. *Fuel* 291, 120129. doi:10.1016/j.fuel.2021.120129

Zhai, C., Jin, Y., Nishida, K., and Ogata, Y. (2021). Diesel spray and combustion of multi-hole injectors with micro-hole under ultra-high injection pressure—non-evaporating spray characteristics. *Fuel* 283, 119322. doi:10.1016/j.fuel.2020.119322

Zhai, C., Jin, Y., Wu, Q., Nishida, K., and Ogata, Y. (2021). Diesel spray and combustion of multi-hole injectors with micro-hole under ultra-high injection pressure—combustion characteristics. *Fuel* 300, 120949. doi:10.1016/j.fuel.2021.120949

Zhang, J., Tang, M., Menucci, T., Schmidt, H., Lee, S-Y., Naber1, J., et al. (2017). "Experimental investigation of spray characteristics of high reactivity gasoline and diesel fuel using a heavy-duty single-hole injector, Part II: Non-reacting, vaporizing sprays," in ILASS americas 29th annual conference on liquid atomization and spray systems, Atlanta, GA, April 2017.

Zhao, L., Torelli, R., Zhu, X., Scarcelli, R., Som, S., Schmidt, H., et al. (2017). An experimental and numerical study of diesel spray impingement on a flat plate. *SAE Int. J. Fuels Lubr.* 10, 422. doi:10.4271/2017-01-0854